ELSEVIER

Journal of Archaeological Science 33 (2006) 1617–1627

Journal of Archaeological SCIENCE

http://www.elsevier.com/locate/jas

Multivariate visualization and analysis of photomapped artifact scatters

Nathan Craig [a,*], Mark Aldenderfer [b], Holley Moyes [c]

[a] Department of Anthropology, University of California, HSSB 2001, Santa Barbara, CA 93106-3210, USA
[b] Department of Anthropology, University of Arizona, Emil W. Haury Building, P.O. Box 210030, Tucson, AZ 85721-0030, USA
[c] Department of Anthropology, State University of New York at Buffalo, 380 MFAC, Ellicott Complex, Buffalo, NY, USA

Received 1 October 2005; received in revised form 24 February 2006; accepted 27 February 2006

Abstract

Simultaneous analysis of relationships between multiple artifact classes is required for characterization of many types of activity areas. This paper illustrates improved forms of multivariate visualization, spatial analysis and integration of experimental results that are possible with GIS based photomapping. Techniques are demonstrated through analysis of a hearth associated artifact scatter exposed during excavations of a Late Archaic pithouse at Jiskairumoko, Peru. A multivariate density raster is created and additive color visualization is used for simultaneous display of three artifact distributions. Performing unconstrained clustering in a GIS, space is classified by simultaneous relative density relationships between multiple object types.

Keywords: GIS; Photomapping; Multivariate density rasters; Unconstrained clustering; Spatial analysis; Experimental archaeology

1. Introduction

Spatial analysis of artifact distributions has been widely used to define and examine activity areas in both archaeological and ethnoarchaeological contexts and represents a well developed intersection of archaeology, ethnography, and quantitative methods. Nowhere has this intersection been more productively articulated than the analysis of household and hearth-based contexts. We build on this foundation by a multivariate analysis of a hearth-associated scatter exposed inside a pithouse.

Specifically, the case study explores hearth based models and applies traditional forms of multivariate and spatial analysis, including correlations, principal components analysis, and factor rotation, as well as unconstrained clustering using both Ward's and k-means classifiers. In doing so we illustrate some shortcomings of these methods and introduce improvements made by possible by construction of a multivariate density mixture raster using geographic information systems (GIS).

2. Jiskairumoko, an early settled village in the Lake Titicaca Basin of the southern Peruvian Highlands

Jiskairumoko is a moderately sized, multi-component open air domestic site located in the upper Rio Ilave, Lake Titicaca Basin, Peru. The site's occupation spans the Archaic to Formative transition. Excavation revealed the presence of a series of Late and Terminal Archaic pithouses as well as two above ground Formative prepared floor structures [10]. When evaluated in a larger context, several of the pit structures from Jiskairumoko are arranged according to a roughly circular layout that is typical of many early villages (Fig. 1).

All of Jiskairumoko's pit houses have well made central interior hearths. A radiocarbon date from the interior hearth in Block 9 dated to 4562 ± 73 BP (AA-58476; 3385-3078 B.C.E). This is the oldest date obtained from any hearth at Jiskairumoko, and currently represents the earliest evidence for reduced residential mobility in the region. Level XIV revealed

* Corresponding author. Tel.: +1 805 893 8604.
E-mail addresses: n8@archaeo.info (N. Craig), aldender@email.arizona.edu (M. Aldenderfer), hmoyes@buffalo.edu (H. Moyes).

0305-4403/$ - see front matter © 2006 Elsevier Ltd. All rights reserved.
doi:10.1016/j.jas.2006.02.018

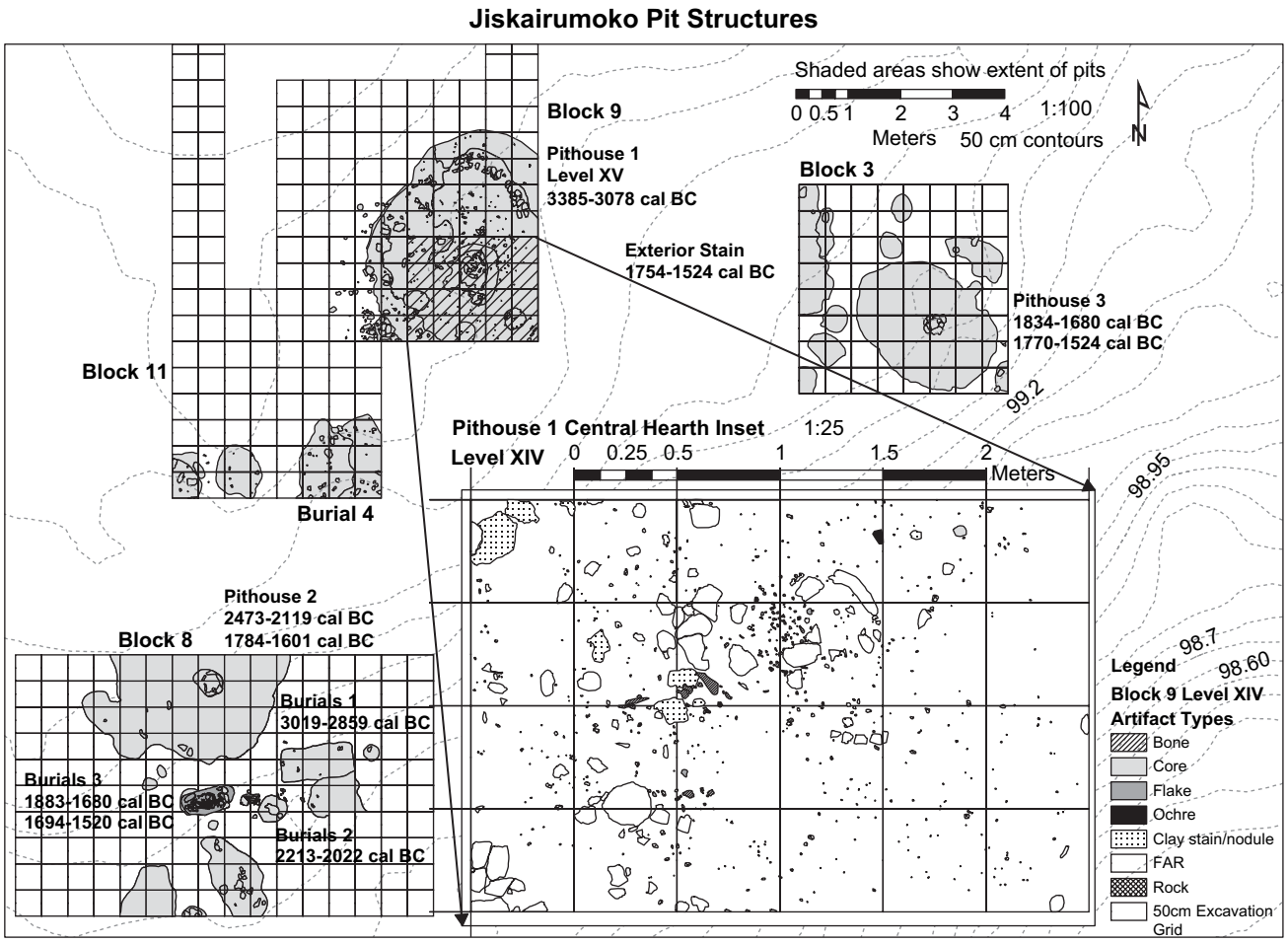

Fig. 1. Circular arrangement of several pit structures from Jiskairumoko that form a small village. Block 9 is shown in the northern portion of this map, the artifact scatter that forms the focus of analysis is illustrated in the inset map.

a scatter of ochre, burned and unburned bone, fine lithic debitage, and fire altered rock (FAR) that rested on the structure's floor that was spatially proximate to the interior hearth. This assemblage serves as the test case for the methods we present (Fig. 1 Inset Map).

The Level XIV hearth associated assemblage probably reflects activities performed relatively early during the structure's occupation. Patterned artifact scatters also occur in the upper levels of material that accumulated in the Block 9 pit structure. These appear to be palimpsest surfaces produced by the structure's re-use. Some (Levels XIII–XI) likely reflect a later occupational use of the structure. Others (Levels X–IV) probably represent various post-abandonment uses of the pit for non-occupational purposes, like the performance of waste producing activities (i.e. butchering and roasting) or secondary disposal.

3. Middle range models relevant to settlement and site formation at Jiskairumoko

The definition of habitation activity areas is difficult to discern because material deposited earlier is often cleaned and deposited elsewhere as secondary refuse. Large artifacts are more likely to be redeposited as trash, but even small artifacts can be disturbed by trampling. In cold environments a wider range of activities should take place inside structures [6: pp. 180–187]. This complicates the identification of refuse associated with discrete activity performance. The performance of more activities in structures leads to more diverse refuse, more rapid refuse accumulation, and thus more frequent cleaning.

Fortunately, activity is structured around the built environment [3: p. 98], cooking hearths, and by the dimensions of the body. As a result, in situ artifacts exhibit strongly identifiable patterns around hearths. The area defined by the mechanics of the arm form an "elementary yardstick" for interpreting spatial patterns [12: p. 252]. Individuals can reach an area of approximately 2.5–3 m^3. A person's reach is about 2.5 m to the front and about 3 m to the rear [11: p. 113].

We conducted seated arm length experiments [c.f. 12: p. 252]. We chose a 1.57 m (5′2″) female because residents of the Titicaca highlands are known for small stature. The subject drew where her buttocks made contact with the ground and transcribed her maximum seated arm length (Fig. 2).

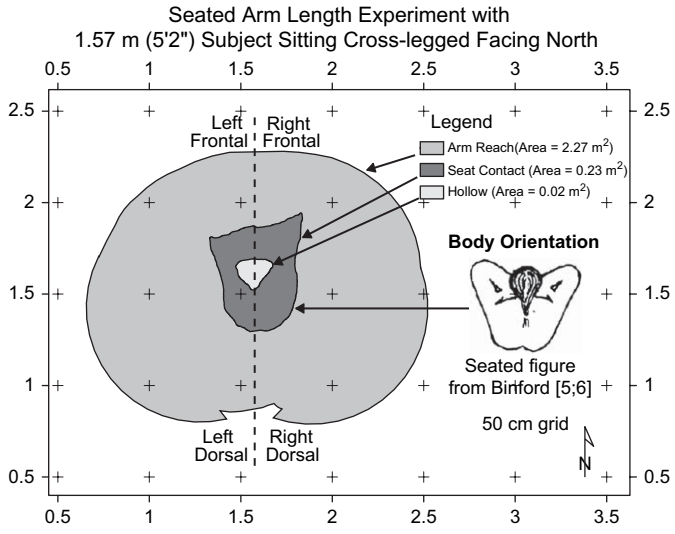

Fig. 2. Seated arm length experiment with a 1.57 m (5′2″) female subject.

Outside hearths are expected to produce drop and toss zones [5: p. 339]. Drop zones occur from about 0.5–1.5 m out from around a hearth, while toss zones range out to about 2–3 m from a hearth. A perpendicular refuse pattern created by a single person habitually sitting at right angles to and within arms reach of a hearth has also been noted [6: pp. 149–151, Figure 85 Hearth D]. According to this model an arc of debris forms in the working surface in front of the person, the hearth is located to one side, and there is a void of refuse located where the person habitually sat.

Hearth associated scatters may also arise as the result of cleaning. This may constitute removal of waste material to secondary dumping areas outside structures [2: p. 285], or it may simply involve scooping out some burned hearth contents and dumping them next to the hearth [13: p. 165, 16].

The context of the Level XIV scatter suggests it could be the product of four possible behavioral processes: drop zone debris, toss zone accumulation, a perpendicular work station, or hearth cleaning. Multivariate visualization and analytical procedures used to identify these processes are described below.

4. Initial observations

The entire excavation of Jiskairumoko was recorded directly into the GIS during excavation through photomapping [9,10]. The photomapped Block 9 Level XIV hearth and its associated scatter are shown in Fig. 3. A total of 712 objects were recorded in this six square meter area (Table 1), and were represented as polygons. The seated arm length experiment was also photomapped and integrated into the GIS.

Visual interpretation of the Level XIV hearth associated scatter suggests that two major artifact groups representing activity areas are present: Zones A and B (Fig. 3). Zone A is a dense concentration of small objects composed primarily of bone, flakes, and ochre. Zone B is composed of the same objects as Zone A but also includes fire altered rock (FAR). The density of artifacts appears to be greater in Zone A than in Zone B, but Zone B appears to have some larger objects.

The Zone A scatter may have been produced by activities taking place around the structure's central hearth or could have resulted from hearth cleaning. Hearth cleaning seems likely for several reasons. Bone and ochre fragments in this concentration show evidence of burning. Furthermore, the concentration of burned bone, ochre, and chert debitage are found within a fine grained ashy soil. The Zone B scatter lies within the expected distance of a drop zone but the area appears to have a lower artifact density than Zone A. Zone B probably represents dropped artifacts rather than hearth cleaning.

While initial observation strongly suggests these two processes, it does not answer two important questions: 1) what is the difference in density and component artifacts making up Zones A and B; and 2) can the differences in zones be defined through quantitatively rigorous techniques rather than visual interpretation?

5. Multivariate analytical procedures for defining activity areas

Like most domestic contexts, artifact scatters from Jiskairumoko consist of multiple artifact classes. Therefore, analytical techniques to define activity areas must permit examination of relationships in the spatial distribution of multiple artifact classes. Unconstrained clustering defines spatial categories based on multivariate vectors of relative densities [22]. Several criteria make unconstrained clustering attractive for application to analysis of photomapped small artifact scatters:

- It is based on density mapping, a technique familiar to most archaeologists and that has been applied in various forms including isoline mapping [1] and local density analysis [15,18,19]. Given the ubiquitous application of density based analysis, results should be easily interpretable by a broad audience.
- Both density mapping, and the map algebra required to create relative densities are easily performed in GIS.
- The technique is based on simultaneous density associations between the spatial distributions of an unlimited number of artifact classes, making it potentially useful for a wide range of other circumstances.
- There is no assumption of a global process conditioning patterning. This is important because a single surface may contain artifacts deposited by performance of multiple activities, and discriminating these differences is often a central cause for analysis.

Unconstrained clustering was initially developed and tested unconstrained clustering through analysis of the Mask Site [5,22], and successfully discriminated drop and toss zones. The technique has subsequently been applied to topics ranging from the spatial distribution of San ceramic motifs [21] to determining the presence of domestic structures in the absence of

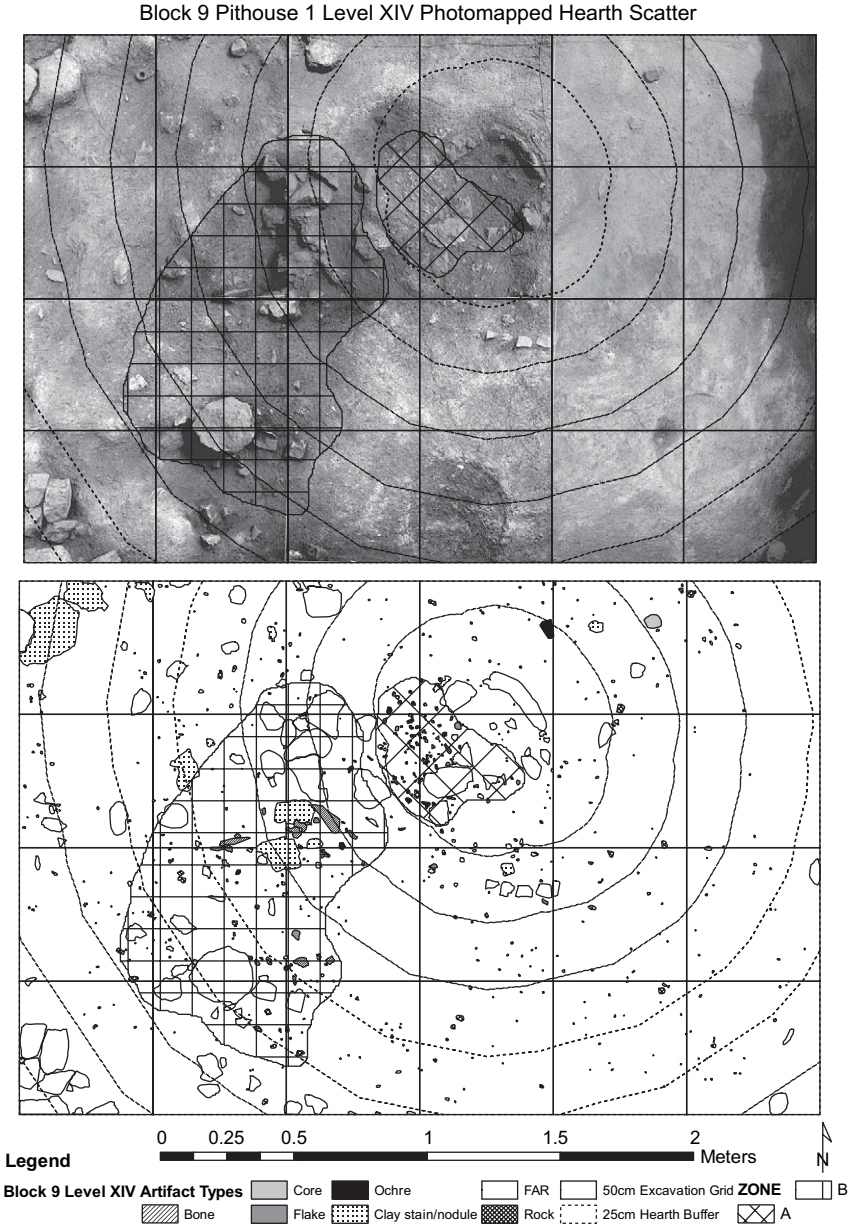

Fig. 3. Upper panel shows high resolution georeferenced photomap with 25 cm buffer around the hearth. Lower panel shows photomapped artifact distribution with 25 cm buffer around hearth.

conventional house remains [17]. Although these applications of unconstrained clustering were performed outside of a GIS, we recognize at least two benefits to be gained by porting this form of spatial analysis to it. First, photomapping facilitates very rapid, high resolution data recording directly into a GIS [9]. Therefore, it would be advantageous to perform analysis in the same system that data is recorded into. Second, an easily applicable technique would facilitate systematic comparisons of different contexts, making photomapped artifact scatters analytically more useful.

Through this approach, we have developed two improvements to unconstrained clustering: the use of multivariate density mixture rasters and a raster approach to clustering, which classifies space rather than artifacts.

Table 1
Number, nearest neighbor statistic, maximum nearest feature (NF) for observed and expected distributions for each artifact class

Object	*N*	*R*	Max NO (m)	Max NE (m)
All other than Clay stain/nodule	302	0.78	–	–
Bone	63	0.3	0.438	0.461
Clay stain/nodule	410	0.769	0.233	0.218
Core	1	NA		
FAR	101	0.85	0.411	0.425
Flake	14	0.26	0.181	1.098
Ochre	20	0.55	1.134	0.308
Rock	101	0.51	0.439	0.318
All	712	0.880	–	–

5.1. Multivariate density mixture rasters

Visualization is an important first step to understanding the structure of a spatial distribution [7,22]. Unfortunately, isopleth mapping only permits effective representation of a single relative density distribution at a time. This makes visual interpretation of relationships between multiple classes problematic.

The generation of relative density rasters in a GIS permits simultaneous representation of three artifact class distributions as red, green and blue multi-band additive false-color composites. Additive false-color composite image display is widely used in multispectral remotely sensed image interpretation to show relationships between different bands of reflected light [14]. Additive color mixture imagery holds great promise for simultaneous representation of up to three artifact class distributions. When these techniques are applied to artifact relative densities we describe them as relative density mixture images because the technique illustrates both distributions and relationships between distributions.

Additive color synthesis is a method of creating color though the mixing of proportions of two, or more commonly three, unique primary stimulus colors. These are nearly always red, green, and blue. For example, images displayed by color televisions are made up of red, green, and blue dots. When observed from a distance, the human eye does not distinguish the dots, and the blending of red, green, and blue dots produces a composite color effect. With additive color raster imagery, three bit-planes representing red, green, and blue exist at every pixel address. Changes in the intensity of illumination on these three bit-planes produce the mixing that leads to the additive color effect [4] (Fig. 4). These principles can be used to interpret variation in density of three rasters simultaneously.

5.2. Classification of activity areas

The final step of unconstrained clustering [22] involves assigning artifacts to clusters that should represent distinct activity areas. Ideally, various clustering algorithms should produce congruent results. At Jiskairumoko, we found that assigning artifacts to categories and attempting to define activity areas from these generated results that were somewhat ambiguous. When using unconstrained clustering in GIS, it is possible to apply clustering algorithms to the multivariate relative density rasters themselves in the same way one would classify a multi-spectral satellite image. Clustering the relative density raster more directly classifies space rather than assigning artifacts to groups and defining spaces based on them. Unconstrained clustering is clearly a powerful method for varied spatial classification applications, and we believe many will find our additions an improvement. For clarity Fig. 5 represents a flowchart of procedures. Steps numbered in the figure correspond to numbers provided in the following narrative description of the methods.

(1) When performing unconstrained clustering in a GIS one can begin by computing a density surface for each class of artifact. We used the maximum nearest feature for the search radius because this permits the creation of the most spatially fine densities possible while simultaneously ensuring that there are no densities composed of single objects.

(2) Once density rasters have been computed, use the GIS to identify the sum of values for each individual artifact density raster. We used ESRI ArcMap 9.1 and the Spatial Analyst extension to perform density analysis and map algebra. Whallon's formula for computing relative density expressed in map algebra is as follows:

$$(([\text{artifact\_class}]/\text{sum of } [\text{artifact\_class}]) \times 100)$$

The resulting output is the percent total or relative density raster.

(3) To classify artifacts according to traditional unconstrained clustering procedures, use the Summarize Zones feature in the Spatial Analyst extension to query either photomapped polygons or polygon centroids against each relative density rasters. If using polygons, join the mean of relative densities inside the polygon; if using points join the cell value of the pixel where each point resides on each relative density raster.

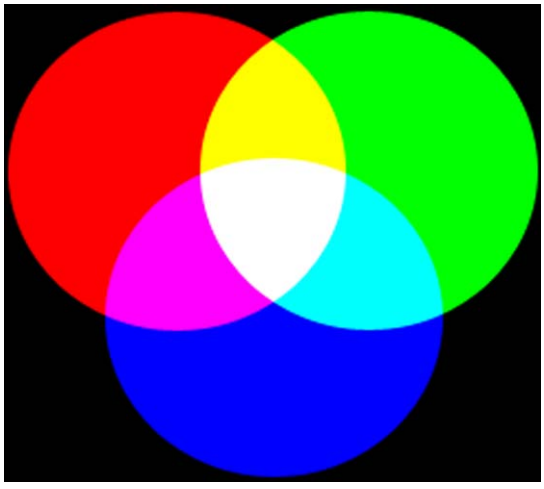

Fig. 4. Fundamentals of additive color theory.

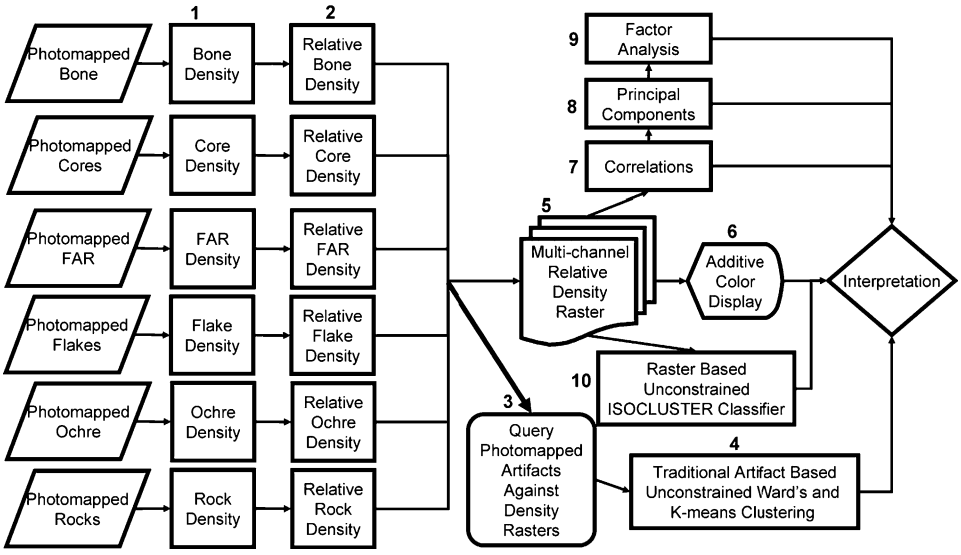

Fig. 5. Multivariate analysis flowchart. Numbers in figure correspond to numbers in narrative description of the method.

(4) Once relative density values are joined to artifacts export the attribute table and use a statistical package to produce clusters. We used polygon representations of artifacts and compared Ward's and K-means algorithms. The JMP 5.1 software package was used for statistical analysis. After clusters were assigned the group assignments were joined in the GIS and the various distributions were displayed to evaluate differences in the cluster solutions.

(5) To follow our modification of unconstrained clustering, assemble all of the relative density rasters into a single multichannel image using the Stack Image function in the Image Analysis extension for ArcView3.X.

(6) The resulting multi-channel raster is a relative density mixture image that can be used for simultaneous display of up to three artifact classes using additive color theory.

Based upon this image, it is possible to calculate correlations between density rasters (7), compute principal components (8) and perform factor analysis (9), and produce a spatial classification using the iterative self-organizing clustering (ISOCLUSTER) classification algorithm [20]. ISOCLUSTER (10) is commonly used for unsupervised classification of multispectral satellite data, though it is simply another kind of clustering algorithm that is broadly similar to k-means. The number of clusters is established beforehand and the ISOCLUSTER algorithm makes iterations through the raster data array until the number of pixels that change groups during an iteration is less than the given threshold.

6. Results and discussion

Artifact counts, nearest neighbor values, and maximum distance to the nearest like artifact for observed (Max NO) and expected (Max NE) distributions of each artifact class are reported in Table 1. Considered as a whole, the distribution is aggregated. Flakes and bone are the most aggregated classes, ochre fragments and rocks are somewhat less aggregated, while clay nodules and FAR are the least aggregated. Since clay nodules are ubiquitous and lack clear spatial patterning, they were excluded from further analysis. FAR was not excluded because this class forms the hearth.

Artifact aggregations break the assumption of a normal distribution, resulting in correlation matrices and principal components of limited value. Regardless, these techniques remain useful for understanding multivariate patterning, and have been used successfully with aggregated data provided caution is exercised. Correlations in the relative density values between artifact classes are reported in Table 1. Principal components and varimax rotated factors produced from these correlations are provided in Tables 2 and 3.

Table 3 shows strong positive correlations between bone, flake, ochre, and rock. There is also a very weak trend toward negative association between these artifacts and FAR. Table 3 indicates a low eigenvalue for PC1 confirming suspicions that there is no global process conditioning patterning. PC1 describes slightly more than half the variability present in the relative density vectors. Consistent with the correlation matrix, the eigenvalues reveal positive associations in relative densities of rocks, bone, ochre, and flakes. PC2 only explains about 20% of the variability and is essentially loaded by a single eigenvalue for FAR. Very low eigenvalues for PC3 suggest little valuable information is expressed by this vector.

Table 4 provides a factor rotation of the first two principal components. Rotation greatly increased eigenvector loadings

Table 2
Correlation coefficients for values obtained from querying each artifact class against each of the relative density rasters

	Bone	FAR	Flake	Ochre	Rock
Bone	1.000				
FAR	−0.031	1.000			
Flake	**0.634**	0.198	1.000		
Ochre	**0.758**	0.149	**0.642**	1.000	
Rock	**0.840**	0.173	**0.780**	**0.744**	1.000

Table 3
Principal components analysis produced from correlations of relative densities

Eigenvalues	**3.229**	**1.020**	0.3823	0.2576	0.111
Percent	64.584	20.396	7.645	5.1526	2.222
Cum Percent	64.584	84.981	92.626	97.779	100.000
Eigenvectors					
Bone	**0.497**	−0.255	0.294	0.488	0.603
FAR	0.000	**0.962**	0.165	0.140	0.123
Flake	**0.476**	0.089	**−0.776**	−0.303	0.269
Ochre	**0.489**	−0.030	**0.525**	−0.687	−0.116
Rock	**0.525**	−0.011	−0.098	0.423	−0.732

again showing rocks, bone, ochre, and flakes occur together in Factor 1. This factor does not explain relative density variability in FAR. Factor 2 explains relative density variability in FAR, but not the other artifact classes.

The application of various hierarchical clustering algorithims produced aggregation distances that suggested a major threshold at a 3 to 4 cluster solution. This result is generally consistent with our visual interpretation of the scatter. Fig. 6 illustrates results from a traditional approach to unconstrained clustering providing both a 3 and 4 cluster solution comparing Ward's and k-means algorithms. Evaluation of artifact cluster assignments in relation to direct observations from the photomosaic in Fig. 3 are not promising. Two troublesome areas labeled Areas 1 and 2 have been identified in Fig. 6 and are annotated by a dashed line.

Area 1: Artifacts within Area 1 were assigned to three groups in each of the potential solutions provided in Fig. 6. All of the objects within Area 1 are probably either part the hearth's drop zone, the hearth itself, or reflect hearth cleaning activities. The latter two are the most likely and are easily distinguishable based on size. The large fragments of FAR clearly make up the hearth while the smaller artifacts were either material cleaned from the hearth or are part of its drop zone. Traditional unconstrained clustering does not appear to be classifying artifacts in a particularly helpful way. An additional complication is the fact that the small alignment of rocks to the south of Area 1 is assigned to different groups in each case, making it difficult to determine how these objects relate to expected activity areas.

Area 2: Fire altered rocks within Area 2 are assigned to three different groups in all versions except for a Ward's three cluster solution. Our interpretation of the photomosaic suggests this rock concentration is part of Zone B. The fact that these objects are assigned to three different groups that are dispersed throughout the analytical space complicates, rather than elucidates, interpretation.

Fig. 7 presents our analysis of the additive false-color composites produced from the relative density mixture image created during our GIS modification of unconstrained clustering. In Fig. 7a, note that ochre, represented as red, is distributed in a circular pattern around the hearth. There is another concentration of ochre just to the west of the hearth and to the north of Area 1. Flakes, represented as green, are only present around the hearth, just to the north and to the east of Area 1. Bone fragments, represented as blue, are distributed in an arc-like pattern from around the western edge of the hearth continuing southward.

Table 4
Varimax rotated factors produced from principal components analysis

Bone	**0.920**	−0.139
FAR	0.067	**0.990**
Flake	**0.836**	0.200
Ochre	**0.874**	0.084
Rock	**0.937**	0.112

Fig. 7b shows FAR represented as red, and illustrates locations to the east of the hearth where FAR is located in areas having low relative densities of either bone or rock. Other locations away from the hearth are also visible as red patches. Bone, represented as green, can be seen mixing with both FAR and rock to the west of the hearth and north of Area 1 producing a white patch. Bone is also mixing in other areas represented as white or magenta.

Fig. 7c shows there are a number of places where FAR is located in low density areas of clay nodules as well. However, there is some mixing with the other two artifact categories around the hearth to the south of Area 1 and around Area 2. Clay, represented as green, is distributed in a number of locations where either FAR or rocks are absent, though there is some mixture between clay and FAR in the two regions already mentioned. Clay and rock have overlapping relative densities in the south-western portion of the image directly west of the figure label. This area is a mixture of clay and rock expressed as magenta.

Fig. 7d illustrates the application of an ISOCLUSTER five class solution to the relative density mixture image, displays the assignment of artifacts to five clusters based on the relative densities of other artifact classes, and shows one possible placement of our seated arm length experiment. Like k-means, ISOCLUSTER requires the analyst assign the number of clusters a priori. Unfortunately, neither Erdas IMAGINE nor ArcMap GIS reports cluster distances for solutions with different numbers of groups. Regardless of this shortcoming, comparing the application of several hierarchical clustering methods to relative density values attached to the artifact tables indicated a clear break in cluster distances of three or four groups.

A five cluster solution with the ISOCLUSTER method produced results that closely replicated our visual interpretation. The five cluster solution was chosen because ISOCLUSTER assigns every pixel to a group, and therefore Cluster 1 represents the "background" cluster. As a result, an ISOCLUSTER five cluster solution is similar to a k-means four cluster solution.

Fig. 8 illustrates the area and artifact density (count/area) within each ISOCLUSTER cluster. Cluster 5 closely approximates Zone A and holds by far the greatest density of all artifacts except FAR. Clusters 3 and 4, which are largely situated on the margins of Cluster 5, are areas of decreasing artifact density. A single patch of Cluster 3 is located to the southwest in Cluster 2. Cluster 2 coincides closely with Zone B and is an area of greater density than Clusters 1–3 but occupies a much larger area than these clusters. Cluster 1 is the lowest density space but covers the greatest area because it is the "background".

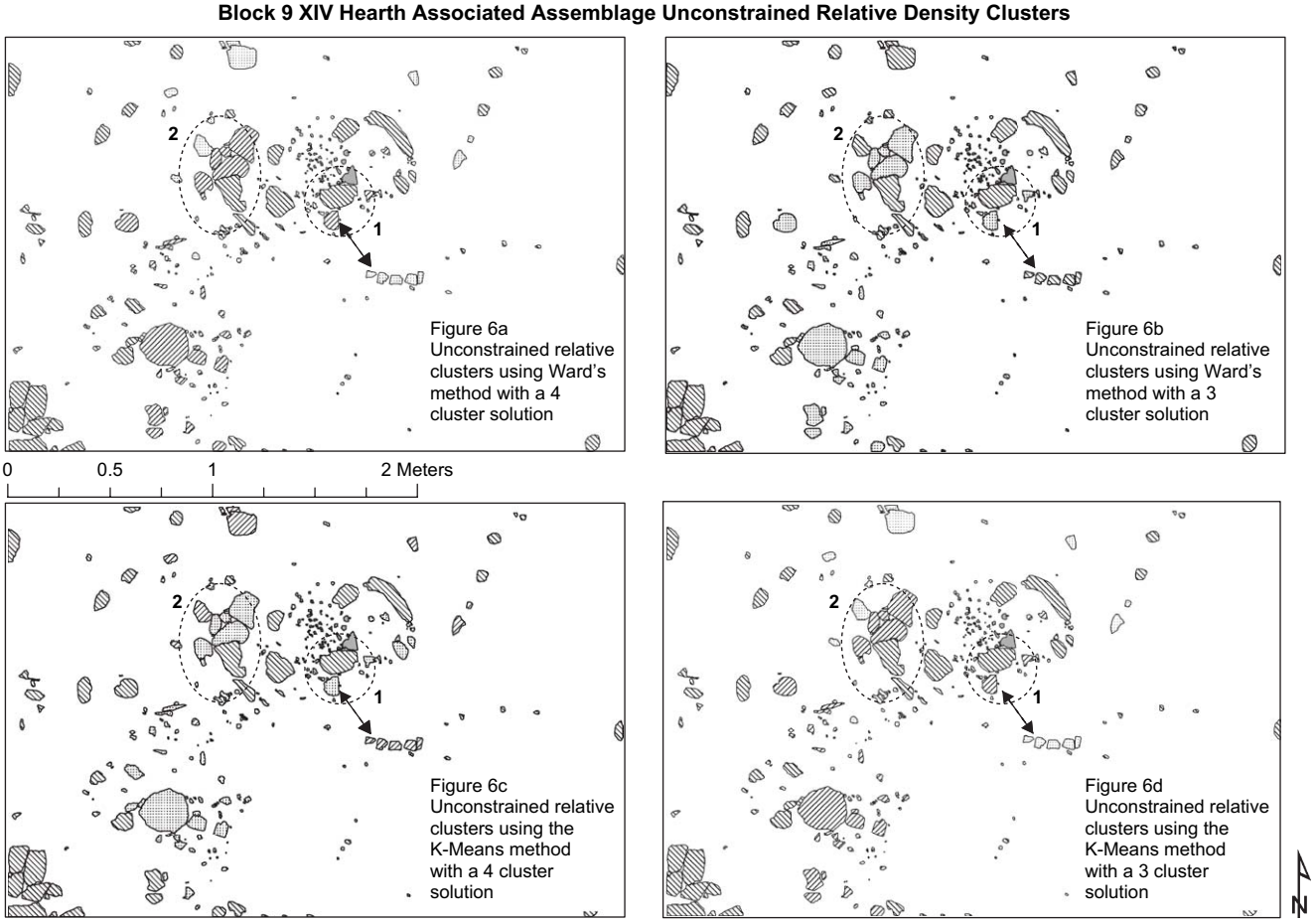

Fig. 6. a–d. Two areas of interest are annotated as 1 and 2 on each cluster solution map. Rocks are assigned to three different clusters in Area 1. In Area 1 one can also see that in each cluster solution map the small alignment of rocks has been assigned to different clusters. Area 2 of each cluster solution is divided into at least two but usually three clusters.

Artifacts in Area 1 have again been assigned to multiple clusters (Clusters 2–5). The spatial pattern of these groups, and their density composition, is markedly easier to interpret than those created by clustering artifacts. The spatial arrangement of clusters created using the ISOCLUSTER classifier are arranged in varying density among spatially correlated artifacts giving them a logical order. The three highest density groups (Clusters 3–5) are arranged concentrically reflecting regions of increasing relative densities among bone, rocks, flakes, and ochre. Therefore the assignment of artifacts in Area 1 to multiple groups illustrates their position with regard to decaying artifact density on the margins of the activity area.

Examining Area 2, one can see that all objects are assigned to Cluster 2 or sit on the edge of Cluster 2. This cluster corresponds closely to Zone B. Objects in Area 2 that are on the edge of Cluster 2 or are located in Cluster 1 are on the margin of this activity area where artifact density is declining. Visually it is easy to recognize that objects on the boundary of the Cluster 2 are probably members of this activity area.

Fig. 7d also shows one possible placement of our seated arm length experiment in a coordinated pattern with the unconstrained ISOCLUSTER results. It illustrates how the perpendicular habitual individual worker model can form a parsimonious explanation of the data. Zone B forms the perpendicular arc that composes the work surface, and Zone A is a specific hearth cleaning/sifting deposit that is probably related to ochre heat treatment.

7. Conclusion and relevance

Quantitative spatial analysis does not yield a direct definitive answer regarding the activities that produced the artifact distributions corresponding to Zones A and B. Contextual information is clearly critical for robust interpretation. Knowing that the Zone A distribution sits upon a lens of fine ashy sediment is an important clue that it represents hearth cleaning rather than a drop zone. Raster based unconstrained clustering procedures helped to classify and segregate ISOCLUSTER Cluster 5 by defining its compositional constituents using quantitative, rather than purely judgmental, criteria. ISOCLUSTER Cluster 2 conforms remarkably well to Zone B and reflects the general spatial and artifact density expectations of a perpendicular workspace. Observations during excavation and display of the photomapped data hinted that such a pattern existed. Application of unconstrained clustering of density rasters in a GIS context again provided a simple and

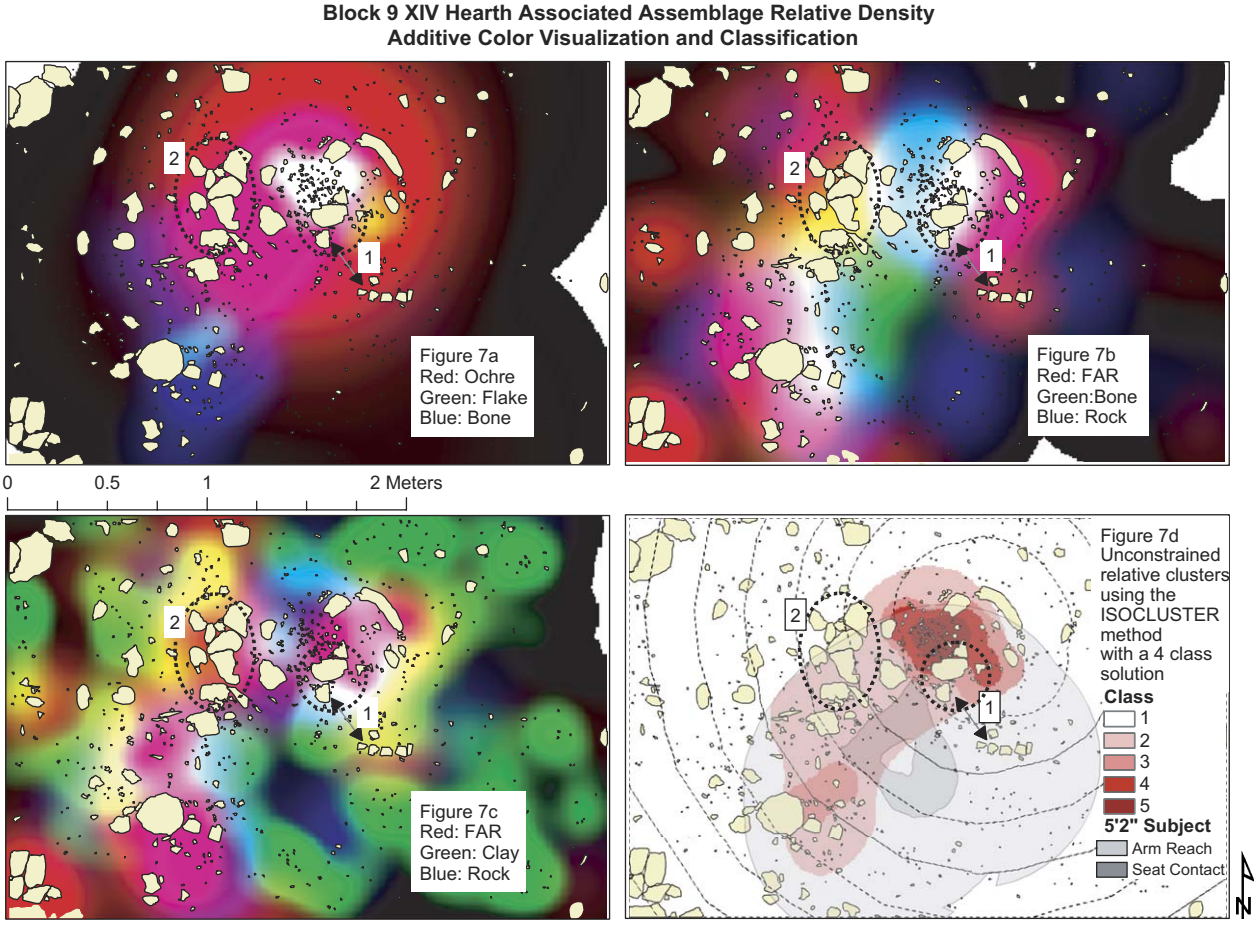

Fig. 7. a–c. Are false color composite images each visualizing the relative densities of three distinct artifact categories as red, green, and blue. Color ranges represent regions of relative density mixture or overlap between the different classes represented in an image. Patterns of color mixture follow additive color theory. For example, purple is a mixture of red and blue. Yellow is a mixture of red and green, and white regions are an equal mixture of red, green, and blue. Fig. 7d illustrates unconstrained relative clusters applied to the relative density surfaces using the ISOCLUSTER method with a four class solution along with 25 cm contour intervals from the hearth.

powerful means to classify and define the constituents of this space on a quantitative basis.

As an initial step in performing unconstrained clustering in a GIS, relative density mixture images can be easily produced, and are extremely useful for visualization during early stages of the analytical process because multi-channel additive color display allows the interpreter to see relationships between distributions of interest. Visualization of complex data sets

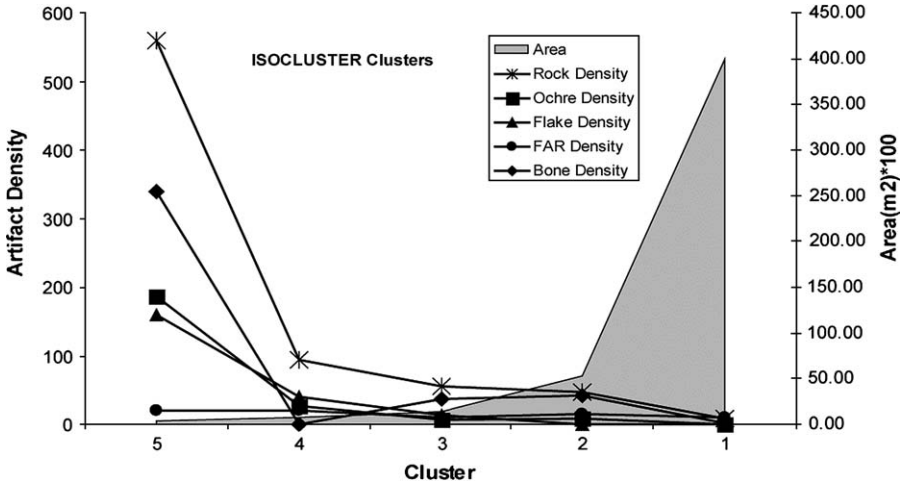

Fig. 8. Graph showing the area and artifact density within each of the ISOCLUSTER clusters.

generated through photomapping can readily be constructed through raster based density analysis. Principal components and factor analysis are also easily performed on relative density mixture images in GIS. At both survey and site scales of analysis, humans produce aggregated residues that are often not conditioned by a single global process. In this case two processes, habitual perpendicular cooking/heating and hearth cleaning, probably structure data patterning. Nonetheless, correlation and principal components analysis yield analytically useful exploratory results.

Clustering space based on raster relative densities is a distinctly different approach than traditional forms of unconstrained clustering. Instead of assigning artifacts to groups and then defining areas based on those groups, areas are defined spatially pixel by pixel based on the density of objects. This is a powerful addition to a well established technique. Since every relative density pixel is included in the clustering process, groups are constructed on a complete sample of space interpolated from observed artifact locations. Segregating space based on the clustering of artifacts relies on a much smaller sample than what can be achieved with purely raster solutions. In this case, clustering based on photomapped objects yields a sample of only 712 entity vectors for classification purposes. In the raster example each relative density raster has an extent of 263 × 381 pixels meaning 100,203 entity vectors were assigned to clusters providing a far finer resolution classification of space.

Fourier transforms, spatial filters, and spectral analysis have all been prescribed for decomposing complex palimpsest depositional sets [8]. These techniques are common multi-spectral analysis techniques and should be easily performed in remote sensing software. Application of these transformations to multivariate artifact density distributions represents an important avenue for future consideration.

GIS based photomapping is a useful and flexible set of tools for integrating experimental data into the interpretation process. Behavioral models can have tremendous heuristic power when used in conjunction with quantitative techniques. In this case they helped recognize and define a Late Archaic domestic hearth side habitual workstation. Meat and bone was processed here, and ochre was heat treated. Since ochre is used exclusively in symbolic contexts at Jiskairumoko [10: pp. 688–693], results presented here indicate that preparation for ritual activity was embedded in domestic tasks.

As various strands of archaeological theory increasingly emphasize the importance of recognizing the actions of individuals or small groups, we conclude that the scale of exposure and resolution of recording will both likewise need to increase. Use of GIS for site level excavation recording through photomapping represents an important new strategy for rapidly achieving this kind of exceptionally high resolution data recording. In this article we have illustrated some multivariate visualization and analytical methodologies for working with complicated piece plotted assemblages generated by this new GIS based documentary approach. We hope others can benefit from the documentary power of photomapping, apply additive color multivariate visualization, take advantage of expanded multivariate raster transformations available in GIS, and continue with the process of seeking evidence of individuals in the archaeological record. Hopefully what we present here stimulates others to apply similar techniques to documentation and analysis of excavations and experiments.

Acknowledgement

Fieldwork at Jiskairumoko in was supported by National Science Foundation grant SBR-9816313 in 1998, and a supplement for fieldwork in 2002; National Science Foundation Equipment Grant SBR-9978006; and a John H. Heinz II Charitable Trust in 1997 and 2002. All grants were awarded to Aldenderfer. The authors would like to thank Sara Abraham for serving as our 5′2″ subject.

References

[1] M.S. Aldenderfer, Montane Foragers Asana and the South-Central Andean Archaic, University of Iowa Press, Iowa City, 1998.
[2] K.M. Ames, D.F. Raetz, S. Hamilton, C. McAfee, Household archaeology of a Southern Northwest Coast Plank House, Journal of Field Archaeology 19 (1992) 275–290.
[3] L.E. Bartram, E.M. Kroll, H.T. Bunn, Variability in camp structure and bone food refuse patterning at Kua San Hunter-Gatherer Camps, in: E.M. Kroll, D.T. Price (Eds.), The Interpretation of Archaeological Spatial Patterning, Plenum, New York, 1991, pp. 77–148.
[4] J.C. Beatty, Raster graphics and color, The American Statistician 37 (1983) 60–75.
[5] L. Binford, Dimensional analysis of behavior and site structure: learning from an Eskimo hunting stand, American Antiquity 43 (1978) 330–361.
[6] L. Binford, In Pursuit of the Past: Decoding the Archaeological Record, Thames and Hudson, New York, 1983.
[7] C. Carr (Ed.), The Nature of Organization of Intrasite Archaeological Records and Spatial Analytic Approaches to their Investigation, Academic Press, New York, 1984.
[8] C. Carr, Alternative models, alternative techniques: variable approaches to intrasite spatial analysis, for concordance in archaeological analysis, in: C. Carr (Ed.), Westport Publishers, Kansas City, MO, 1985, pp. 302–473.
[9] N. Craig, Real-time GIS construction and digital data recording of the Jiskairumoko Excavation, Peru, SAA Bulletin 18 (2000) 1–10.
[10] N. Craig, The Formation of Early Settled Villages and the Emergence of Leadership: A Test of Three Theoretical Models in the Rio Ilave, Lake Titicaca Basin, Southern Peru, Anthropology, University of California at Santa Barbara, Santa Barbara, 2005, p. 995.
[11] L.G. Freeman, The analysis of some occupation floor distributions from earlier and middle Paleolithic sites in Spain, in: L.G. Freeman (Ed.), Views of the Past, Mouton Publishers, Paris, 1982, pp. 57–116.
[12] C. Gamble, The Paleolithic Settlement of Europe, Cambridge University Press, New York, 1986.
[13] J.A.J. Gowlett, High definition archaeology: ideas and evaluation, World Archaeology 29 (1997) 152–171.
[14] J.R. Jensen, Introductory Digital Image Processing: a Remote Sensing Perspective, Prentice Hall, Upper Saddle River, 1996.
[15] G.A. Johnson, Organizational structure and scalar stress, in: C. Renfrew, M. Rowlands, B.A. Segraves (Eds.), Theory and Explanation in Archaeology, Academic Press, New York, 1982, pp. 289–421.
[16] A. Leroi-Gourhan, Les Religions de la Préhistoire, Presses Universitaires, Paris, 1964.

[17] B. Logan, M.E.J. Hill, Spatial analysis of small scale debris from a late prehistoric site in the lower Missouri Valley, Kansas, Journal of Field Archaeology 27 (2000) 241–256.
[18] H. Moyes, The Cave as a Cosmogram: The Use of GIS in an Intrastie Spatial Analysis of the Main Chamber of Actun Tunichil Muknal, A Maya Ceremonial Cave in Western Belize, Anthropology, Florida Atlantic University, Boca Raton, 2001.
[19] H. Moyes, The use of GIS in the spatial analysis of an archaeological cave site, Journal of Cave and Karst Studies 64 (2002) 9–16.
[20] J.A. Richards, Remote Sensing Digital Image Analysis: An Introduction, Springer-Verlag, New York, 1986.
[21] R. Riddings, G.C. Sampson, There's no percentage in it: intersite spatial analysis of Bushman (San) pottery decorations, American Antiquity 55 (1990) 766–780.
[22] R. Whallon, Unconstrained clustering for the analysis of spatial distributions in archaeology, in: H. Hietala (Ed.), Intrasite Spatial Analysis in Archaeology, Cambridge University Press, Cambridge, 1984, pp. 242–278.